Available online at www.sciencedirect.com
SCIENCE DIRECT®
Coordination Chemistry Reviews 249 (2005) 1476–1490
COORDINATION CHEMISTRY REVIEWS
www.elsevier.com/locate/ccr

Review

A comparative study on metal–metal interaction in binuclear two- and three-coordinated d^{10}-metal complexes Spectroscopic investigation of M(I)–M(I) interaction in the $^1[d\sigma^*p\sigma]$ excited state of $[M_2(dcpm)_2]^{2+}$ (dcpm = bis(dicyclohexylphosphino)methane) (M = Au, Ag, Cu) and $[M_2(dmpm)_3]^{2+}$ (dmpm = bis(dimethylphosphino)methane) (M = Au, Ag, Cu) complexes

David Lee Phillips*, Chi-Ming Che**, King Hung Leung, Zhong Mao, Man-Chung Tse

Department of Chemistry and the HKU-CAS Joint Laboratory on New Materials, The University of Hong Kong, Pokfulam Road, Hong Kong

Received 28 July 2004; accepted 21 September 2004
Available online 14 November 2004

This work is dedicated to the memory of Professor Vincent M. Miskowski.

Contents

1. Introduction 1477
2. Experimental methods 1477
3. Computational methods 1478
4. Results and discussion 1479
   4.1. Ultraviolet absorption and resonance Raman spectra of dibridged $[M_2(dcpm)_2]^{2+}$ (M=Au, **1**; Ag, **2**; Cu, **3**) and tribridged $[M_2(dmpm)_3]^{2+}$ (M=Au, **4**; Cu, **5**; Ag, **6**) compounds 1479
   4.2. Resonance Raman intensity analysis of absorption and resonance Raman spectra of dibridged $[M_2(dcpm)_2]^{2+}$ (M=Au, **1**; Ag, **2**; Cu, **3**) and tribridged $[M_2(dmpm)_3]^{2+}$(M=Au, **4**; Cu, **5**; Ag, **6**) compounds 1480
   4.3. Comparison of the force constants and metal–metal separations for the ground electronic state and the excited $^1[d\#\sigma^*p\#\sigma]$ electronic state for dibridged $[M_2(dcpm)_2]^{2+}$ (M=Au, **1**; Ag, **2**; Cu, **3**) and tribridged $[M_2(dmpm)_3]^{2+}$ (M=Au, **4**; Cu, **5**) compounds with those for other Au, Ag, and Cu dimer compounds 1484
5. Concluding remarks and future prospects 1489
   Acknowledgments 1490
   References 1490

Abstract

An overview of an UV–vis spectroscopic and resonance Raman investigation of the lowest energy dipole-allowed absorption band of $[M_2(dcpm)_2]^{2+}$ (M = Au, Ag, Cu) and $[M_2(dmpm)_3]^{2+}$ (M = Au, Ag, Cu) complexes is presented. The UV–vis absorption spectra of $[M_2(dcpm)_2]^{2+}$ and $[M_2(dmpm)_3]^{2+}$ feature intense low energy $nd\sigma^* \rightarrow (n+1)p\sigma$ transition with transition energy increase from two- to three-coordinated complexes and for $[M_2(dcpm)_2]^{2+}$ falls in the order: Ag > Au > Cu. A resonance Raman intensity analysis of the spectra

* Corresponding author. Tel.: +852 2859 2160; fax: +852 2857 1586.
** Co-corresponding author.
E-mail addresses: phillips@hku.hk (D.L. Phillips), cmche@hku.hk (C.-M. Che).

doi:10.1016/j.ccr.2004.09.015

allows estimation of the structural changes of the $^1[d\sigma^*p\sigma]$ excited states relative to the ground state. The structural changes in these compounds are compared with each other and with other related compounds. The metal–metal bonds are found to be very similar for the ground and excited states of the $[Au_2(dcpm)_2]^{2+}$ and $[Au_2(dmpm)_3]^{2+}$ complexes but significantly different for the $[Cu_2(dcpm)_2]^{2+}$ and $[Cu_2(dmpm)_3]^{2+}$ complexes that have weaker metal–metal bonding.

Keywords: Aurophilicity; Copper; Metal–metal interactions; Raman spectroscopy; Silver

1. Introduction

Spectroscopic studies of d^{10}–d^{10} interactions in binuclear metal compounds $[M_2(diphosphine)_2]^{2+}$ (M = Cu, Ag, Au) have shown the presence of a low energy $nd\sigma^* \rightarrow (n+1)p\sigma$ transition that is not present in the mononuclear counterpart compounds [1–11]. Gray and co-workers [5,6] first observed this type of metal–metal transition in d^8–d^8 complexes of Rh(I) and Pt(II). Their studies concluded the occurrence of weak metal–metal interaction in the ground state and a single metal–metal bond formation in the excited states.

In the course of investigation on luminescent gold(I) complexes with bridging phosphine ligands for photo-induced electron transfer reactions [3,12], the prototypical $[Au_2(dppm)_2]^{2+}$ (dppm = bis(diphenylphosphino)methane) compound was found to display a strong $5d\sigma^* \rightarrow 6p\sigma$ electronic transition at 297 nm and a long-lived photoluminescence in solution at 570 nm [3,4,13]. Ab initio calculations done by Zhang and Che [7] showed that the $^3[d\sigma^*p\sigma]$ excited state of $[Au_2(H_2PCH_2PH_2)_2]^{2+}$ has a Au–Au single bond and easily forms a metal–metal bonded solvent/anion exciplex that emits at 331 nm in solution at room temperature. The excited states formed from photoexcitation of the $5d\sigma^* \rightarrow 6p\sigma$ transition of Au(I) binuclear compounds have interesting excited state properties [13,14]; however, the structural change of the $^{1,3}[d\sigma^*p\sigma]$ excited state relative to the ground state is difficult to determine. We have recently demonstrated the utility of resonance Raman intensity analysis to estimate the structural changes of the $^{1,3}[d\sigma^*p\sigma]$ excited states relative to the ground states in $[Au_2(dcpm)_2]^{2+}$ (dcpm = bis(dicyclohexylphosphino)methane) [8]. Subsequently, we have also communicated the spectral assignments of the $nd\sigma^* \rightarrow (n+1)p\sigma$ transitions in binuclear $[Ag_2(dcpm)_2]^{2+}$ [9], $[Cu_2(dcpm)_2]^{2+}$ [10], and $[Au_2(dmpm)_3]^{2+}$ [11] complexes. In this paper, we present a comparative study on the M(I)–M(I) interaction based on UV–vis spectroscopic data and resonance Raman intensity analysis investigation of the lowest energy dipole-allowed absorption band of $[M_2(dcpm)_2]^{2+}$ (M = Au(I), Ag(I), Cu(I)) and $[M_2(dmpm)_3]^{2+}$ (M = Au(I), Cu(I)) compounds. The dcpm and dmpm ligands in these compounds have intraligand transitions that occur at higher energies than the $nd\sigma^* \rightarrow (n+1)p\sigma$ transitions. Our results indicate that the M(I)–M(I) interaction decreases from two- to three-coordinated binuclear complexes and the $[d\sigma^*p\sigma]$ excited states of both $[M_2(dcpm)_2]^{2+}$ and $[M_2(dmpm)_3]^{2+}$ have much stronger metal–metal bonding interaction with a formal metal–metal single bond than the ground states. We estimate the structural changes of the initial $^1[d\sigma^*p\sigma]$ excited state of these compounds and compare their properties to each other.

2. Experimental methods

The preparation and crystal structures of $[Au_2(dcpm)_2](ClO_4)_2$ (**1**) [13], $[Ag_2(dcpm)_2](SO_3CF_3)_2$ (**2**) [9], $[Cu_2(dcpm)_2](ClO_4)_2$ (**3**) [10], $[Au_2(dmpm)_3](ClO_4)_2$ (**4**) [11], $[Cu_2(dmpm)_3](ClO_4)_2$ (**5**) [15] and $[Ag_2(dmpm)_3](SO_3CF_3)_2$ (**6**) [15] are described elsewhere. The resonance Raman experiments used sample solutions with concentrations in the 5–10 mM range for the $[M_2(dcpm)_2]^{2+}$ samples in spectroscopic grade acetonitrile solvent (for M = Au and Ag) or dichloromethane solvent (for M = Cu) and $[M_2(dmpm)_3]^{2+}$ samples in water solvent (for M = Au and Cu). We note that CH_2Cl_2 was chosen as the solvent for M = Cu because the X-ray crystal structures of material crystallized from CH_3CN solution display the cationic species $[Cu_2(dcpm)_2(CNCH_3)_2]^{2+}$ with an CH_3CN molecule bound to each Cu(I) in a T-shaped geometry [10]. Since the solution electronic absorption spectrum in CH_3CN is strongly perturbed from that in CH_2Cl_2 [10], adducts are also presumably present in CH_3CN solution. There is however, no evidence for strong CH_3CN ground state complexation for M = Au(I) or Ag(I) and CH_3CN was chosen as the solvent for these complexes because of relatively poor photochemical stability in CH_2Cl_2 solvent. Only a brief description is presented here for the resonance Raman apparatus and methods since they have been previously described [8–10,16–20]. The harmonics and hydrogen Raman shifted laser lines from a Nd:YAG laser provided the excitation frequencies for the resonance Raman experiments. A loosely focused laser beam (~1 mm diameter) excited the samples and ~130° backscattering geometry was used to collect the Raman scattering using reflective optics. The Raman light was then imaged through a depolarizer, the entrance slit of a 0.5 m spectrograph, which dispersed the light onto a liquid nitrogen-cooled CCD detector. Scans of about 1–2 min were collected from the CCD and approximately 30–60 of these scans were summed to find the resonance Raman spectrum.

Known acetonitrile, dichloromethane, and water solvent bands as well as Hg lamp emission lines were used to calibrate

the Raman shifts of the resonance Raman spectra. The resonance Raman spectra were intensity corrected for sample reabsorption and the wavelength dependence of the detection system response [21]. Suitably scaled solvent and quartz cell background spectra were subtracted in order to remove the solvent bands, the Rayleigh line and the quartz cell background signal from the raw resonance Raman spectra. Segments of the resonance Raman spectra were fit to a baseline plus a sum of Lorentzian bands to get the integrated areas of the Raman bands.

The absolute resonance Raman cross-sections of the $[M_2(dcpm)_2]^{2+}$ and $[M_2(dmpm)_3]^{2+}$ complexes were measured relative to the absolute Raman cross-sections of acetonitrile, water and dichloromethane solvent bands [17,22,23]. The concentrations of the sample solutions were determined spectrophotometrically using a UV–vis spectrometer (changes of less than 5% were observed for the absorption spectra during the absolute Raman cross-section measurements). The absolute resonance Raman cross-sections were computed from the mean of a series of measurements. The absolute resonance Raman cross-sections displayed little power dependence over a range of 0.1–1.5 mW (differences of <5% were observed). The maximum molar extinction coefficient was determined to be 28,900 M^{-1} cm^{-1} for the ~278 nm absorption band of $Au_2(dcpm)_2(ClO_4)_2$ in acetonitrile solution, 17,000 M^{-1} cm^{-1} for the ~261 nm absorption band of $Ag_2(dcpm)_2(SO_3CF_3)_2$ in acetonitrile solution, 14,090 M^{-1} cm^{-1} for the ~311 nm absorption band of $Cu_2(dcpm)_2(ClO_4)_2$ in dichloromethane solution, 18,500 M^{-1} cm^{-1} for the ~256 nm absorption band of $Au_2(dmpm)_3(ClO_4)_2$ in water solution, 10,800 M^{-1} cm^{-1} for the ~276 nm absorption band of $Cu_2(dmpm)_3(ClO_4)_2$ in water solution, and 6400 M^{-1} cm^{-1} for the ~260 nm absorption band of $Ag_2(dmpm)_3(SO_3CF_3)_2$ in water solution.

3. Computational methods

The calculations presented here are meant to obtain a reasonable estimate of the structural changes associated with the dσ* → pσ transitions of the complexes examined. The results given here will also provide a useful reference to which more sophisticated simulations can be compared to assess the relative importance of effects like changes in the transition dipole moment with vibrational coordinate and anharmonicity on the resonance Raman and absorption spectra. The resonance Raman intensities and absorption spectra were calculated using a time-dependent formalism [24–34]. The absorption cross-sections were calculated using:

$$\sigma_A(E_L) = \frac{4\pi e^2 E_L M^2}{3n\bar{h}^2 c} \int_{-\infty}^{\infty} d\delta\, G(\delta) \sum_i P_i \,\mathrm{Re}\left[\int_0^{\infty} \langle i|i(t)\rangle \times \exp\left[\frac{i(E_L+\varepsilon_i)t}{\bar{h}}\right] \exp[-g(t)]\, dt\right] \quad (1)$$

The resonance Raman cross-sections were computed using the following equation:

$$\begin{aligned}\sigma_R(E_L,\omega_s) &= \int_{-\infty}^{\infty} d\delta\, G(\delta) \sum_i \sum_f P_i \sigma_R(E_L) \delta(E_L + \varepsilon_i - E_S - \varepsilon_f) \quad \text{with} \quad \sigma_{R,i\to f}(E_L) \\ &= \frac{8\pi e^4 E_S^3 E_L M^4}{9\bar{h}^6 c^4} \left| \int_0^{\infty} \langle f|i(t)\rangle \times \exp\left[\frac{i(E_L+\varepsilon_i)t}{\bar{h}}\right] \exp[-g(t)]\, dt \right|^2 \end{aligned} \quad (2)$$

where n is the solvent index of refraction, M is the transition length evaluated at the equilibrium geometry, E_L is the incident photon energy, E_S is the scattered photon energy, f is the final state for the resonance Raman process, ε_f is the energy of the ground state energy level $|f\rangle$, and $\delta(E_L + \varepsilon_i - E_S - \varepsilon_f)$ is a delta function to sum up cross-sections with the same frequency. P_i is the initial Boltzmann population of the ground state energy level $|i\rangle$ which has energy ε_i. $|i(t)\rangle = e^{-iHt/\bar{h}|i\rangle}$ is $|i(t)\rangle$ propagated on the excited state surface for a time t and H is the excited state vibrational Hamiltonian. The absorption and resonance Raman cross-sections were calculated using a summation over a ground state 298 K Boltzmann distribution of vibrational energy levels. The Condon approximation was used. The ground and excited state potential energy surfaces were simulated by harmonic oscillators displaced by Δ in dimensionless normal coordinates. The time-dependent overlaps in Eqs. (1) and (2) were computed numerically from analytic formulations of Yan and Mukamel [35].

We did computations with the damping function $\exp[-g(t)]$ term in Eqs. (1) and (2) modeled as a simple exponential decay function (where the $\exp[-g(t)]$ term in Eqs. (1) and (2) was replaced by $\exp[-t/\tau]$ with τ the dephasing time) or as a Brownian oscillator. The $g(t)$ function has the following form in Eqs. (1) and (2) for the Brownian oscillator dephasing function:

$$g(t) = \left(\frac{D}{\Lambda}\right)^2 (\Lambda t - 1 + \exp(-\Lambda t)) + i\left(\frac{D^2\Lambda}{2kT}\right) \times (1 - \exp(-\Lambda t)) + \frac{t}{\tau} \quad (3)$$

where the solvent random perturbations cause the solute energy levels to fluctuate with D magnitude and Λ frequency [35,36]. We assumed that that the temperature (T) is large enough that the solvent mode frequencies are $\ll kT$ [18,44] and that all the solvent modes were grouped together into one effective mode. The t/τ term in Eq. (3) is the pure lifetime decay.

4. Results and discussion

*4.1. Ultraviolet absorption and resonance Raman spectra of dibridged $[M_2(dcpm)_2]^{2+}$ (M = Au, **1**; Ag, **2**; Cu, **3**) and tribridged $[M_2(dmpm)_3]^{2+}$ (M = Au, **4**; Cu, **5**; Ag, **6**) compounds*

Fig. 1 shows a sketch of the geometries of the dibridged $[M_2(dcpm)_2]^{2+}$ (M = Au, **1**; Ag, **2**; Cu, **3**) and tribridged $[M_2(dmpm)_3]^{2+}$ (M = Au, **4**; Cu, **5**; Ag, **6**) compounds examined in this work. The metal atoms in the dcpm complexes are two-coordinated and in the dmpm complexes are three-coordinated. All complexes have intramolecular metal–metal distances that allow weak d^{10}–d^{10} metal interaction. The metal–metal distances follow the order: **3** (2.731(2), 2.639(2) Å) [10] < **1** (2.9263(9) Å) [13,14] < **2** (2.936(1), 2.960(1) Å); [9] **5** (3.021(2) Å) [15] ∼ **4** (3.028 Å) [11,37] < **6** (3.036(2) Å) [15]. The Au–Au distance in **4** is slightly longer, i.e. ∼0.1 Å, than that in **1** suggesting that an increase in phosphine coordination around Au(I) has little effect on the metal–metal distance. Similarly, the Ag–Ag distances in **3** and **6** differ only by ∼0.1 Å. In contrast, the Cu_2 distance significantly lengthens from **3** to **5**. Fig. 2 displays the absorption spectra of **1**–**3** in dichloromethane solutions, and **4**–**6** in water solution. The electronic absorption data are listed in Table 1. All these complexes display a lower energy intense absorption band that are absent in the absorption spectra of the mononuclear $M(PR_3)_3^+$ and $M(PR_3)_2^+$ counterparts. These intense absorptions are assigned to $^1[d\sigma^* \rightarrow p\sigma]$ transitions, which is supported by resonance Raman experiments described in latter sections.

The excitation wavelengths (in nm) for the resonance Raman experiments are given in Fig. 3. Figs. 4–6 present an overview of the resonance Raman spectra of **1** and **4**, **2**, and **3** and **5**, respectively, for the excitation wavelengths shown in Fig. 3 for each compound. The resonance Raman spectrum of

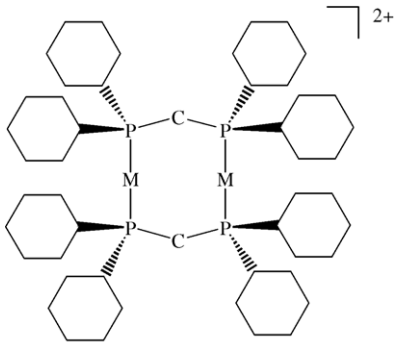

Geometry of $[M_2(dcpm)_2]^{2+}$
where M = Au (**1**), Ag (**2**) and Cu (**3**)

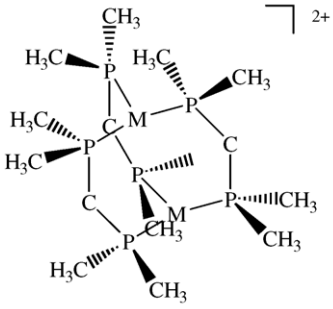

Geometry of $[M_2(dmpm)_3]^{2+}$
where M = Au (**4**) and Cu (**5**)

Fig. 1. Geometry of $[M_2(dcpm)_2]^{2+}$ (where M = Au, **1**; Ag, **2**; Cu, **3**) and $[M_2(dmpm)_3]^{2+}$ (where M = Au, **4**; Cu, **5**).

6 was not recorded due to its instability in solution—one of the dmpm ligands easily dissociates from $[Ag_2(dmpm)_3]^{2+}$ to give $[Ag_2(dmpm)_2]^{2+}$. The resonance Raman spectra shown in Figs. 4–6 display most of their Raman intensity in the nominal metal–metal stretch fundamentals and overtones ($n\nu_{Au-Au}$, $n\nu_{Ag-Ag}$, and $n\nu_{Cu-Cu}$). This is consistent with

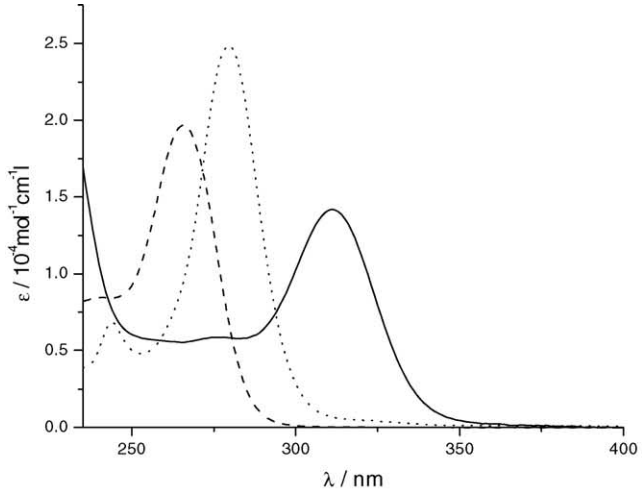

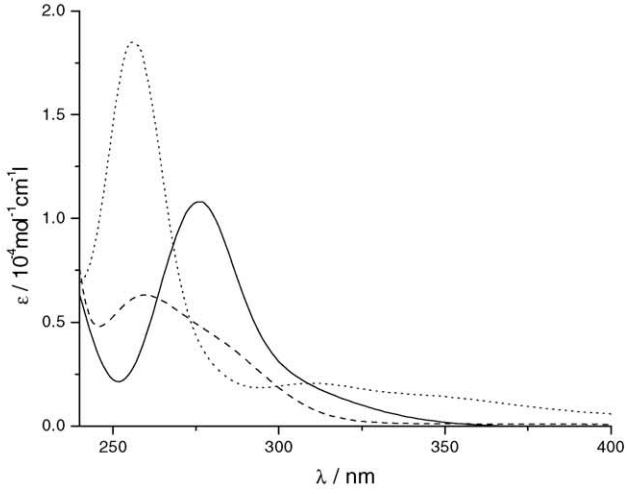

Fig. 2. UV–vis absorption spectra of: (left) $[Au_2(dcpm)_2]^{2+}$ (**1**) (dotted line), $[Ag_2(dcpm)_2]^{2+}$ (**2**) (dashed line) and $[Cu_2(dcpm)_2]^{2+}$ (**3**) (solid line) in dichloromethane solutions; (right) $[Au_2(dmpm)_3]^{2+}$ (**4**) (dotted line), $[Cu_2(dmpm)_3]^{2+}$ (**5**) (solid line) and $[Ag_2(dmpm)_3]^{2+}$ (**6**) (dashed line) in water solutions at room temperature.

Table 1
The UV–vis absorption data

Complex	Medium (298 K)	λ_{abs} [nm] (ε [$dm^3\ mol^{-1}\ cm^{-1}$])
$[Au_2(dcpm)_2](ClO_4)_2$ (**1**)	CH_3CN	278 (28900), 317 (sh[a], 390)
	CH_2Cl_2	280 (24900), 322 (sh[a], 350)
$[Ag_2(dcpm)_2](SO_3CF_3)_2$ (**2**)	CH_3CN	261 (17000)
	CH_2Cl_2	266 (19700)
$[Cu_2(dcpm)_2](ClO_4)_2$ (**3**)	CH_3CN	269 (4830), 319 (4820)
	CH_2Cl_2	278 (5840), 311 (14090)
$[Au_2(dmpm)_3](ClO_4)_2$ (**4**)	H_2O	256 (18500), 311 (1490), 340 (sh[a], 1070)
$[Cu_2(dmpm)_3](ClO_4)_2$ (**5**)	H_2O	276 (10800), 320 (sh[a], 1260)
$[Ag_2(dmpm)_3](SO_3CF_3)_2$ (**6**)	H_2O	260 (6400), 280 (sh[a], 4300)

[a] Shoulder.

the proposed assignments of the excited absorption bands (∼277 nm for **1**, ∼260 nm for **2** and ∼310 nm for **3**) to be due to $d\sigma^* \rightarrow p\sigma$ transitions [8–11]. Table 2 gives the Raman shifts, relative resonance Raman intensities and absolute resonance Raman cross-sections for **1**–**5** obtained from the experimental resonance Raman spectra of Figs. 4–6.

*4.2. Resonance Raman intensity analysis of absorption and resonance Raman spectra of dibridged $[M_2(dcpm)_2]^{2+}$ (M = Au, **1**; Ag, **2**; Cu, **3**) and tribridged $[M_2(dmpm)_3]^{2+}$ (M = Au, **4**; Cu, **5**; Ag, **6**) compounds*

We have modeled the absorption spectra and resonance Raman intensities of **1**–**5** using time-dependent wavepacket computations in order to estimate the structural change of the excited state relative to the ground state. In our initial works on **1** [8] and **4** [11] and the well-studied $[Pt_2(P_2O_5H_2)_4]^{4+}$ [19], we demonstrated that computations using a simple exponential decay function or an overdamped Brownian oscillator function to simulate the solvent dephasing gave very similar fits to the experimental data and almost the same values for the normal mode displacement parameter and excited state frequency of the metal–metal stretch mode. The two types of calculations (simple exponential damping function or overdamped Brownian oscillator function) gave similar values for the other best-fit simulation parameters with some differences that could be attributed to the different lineshapes of the two types of computations [8,19]. Since the overdamped Brownian oscillator function for the solvent dephasing gives a somewhat more realistic description that can account for solvent reorganization and the Stokes shift between absorption and emission [24,36], we only present the best-fit parameters for the Brownian oscillator dephasing function calculations in Table 3. Figs. 7–9 present comparisons of the experimental and calculated absorption spectra and relative resonance Raman intensities for **1** and **4**, **2**, and **3** and **5**, respectively. Inspection of Figs. 7–9 reveals there is reasonable agreement between the calculated and experimental absorption spectra and the relative Raman intensities. Table 2 also displays a comparison of the calculated and experimentally determined absolute resonance Raman cross-sections for the first overtone or the fundamental Raman band for **1**–**5**. Examination of Table 2 indicates that there is good agreement between the experimental and calculated absolute resonance Raman cross-sections.

The normal mode parameters given in Table 3 can be used to estimate the metal–metal bond length change in the initial excited state relative to the ground state. Assuming the nominal metal–metal stretch vibration is approximated by a pure metal–metal stretch, the following formula [24] can be used to find the change in the bond length:

$$q = \left(\frac{\mu\omega}{\hbar}\right)^{1/2} \Delta x \quad (4)$$

where q is the dimensionless normal coordinate, μ is the reduced mass of the metal–metal bond, ω is the ground state vibrational frequency and Δx is the change in the bond length relative to the ground state bond length. The bond length changes, in Table 4, were found using the parameters of Table 3 in Eq. (4). For the dibridged compounds, the Δx becomes larger as one goes from the Au complex **1** (0.11 Å) to the Ag complex **2** (0.20 Å) and to the Cu complex **3** (0.28 Å). There is similar behavior for the tribridged compounds with Δx smaller for the Au complex **4** (0.11 Å) compared to the Cu complex **5** (0.20 Å).

Inspection of Tables 3 and 4 shows that the estimated excited state frequencies are similar for all five compounds, which show a sizeable increase in frequency

Table 2
Resonance Raman bands of $[Au_2(dcpm)_2]^{2+}$ (**1**) in acetonitrile solution, $[Ag_2(dcpm)_2]^{2+}$ (**2**) in acetonitrile solution, $[Cu_2(dcpm)_2]^{2+}$ (**3**) in dichloromethane solution, $[Au_2(dmpm)_2]^{2+}$ (**4**) in water solution, and $[Cu_2(dmpm)_3]^{2+}$ (**5**) in water solution

Raman band	Raman shift (cm^{-1})[a]	Intensity[b]			
		266.0 nm	273.9 nm	282.4 nm	299.1 nm
$Au_2(dcpm)_2(ClO_4)_2$ (**1**) (values from [8])					
$-2\nu_{Au-Au}$	−176	9	19	20	20
$-\nu_{Au-Au}$	−88	80	104	164	202
ν_{Au-Au}	88	199	254	309	288
$2\nu_{Au-Au}$	176	100	100	100	100
Experimental		1.4×10^{-8}	2.4×10^{-8}	1.1×10^{-8}	2.6×10^{-10}
Calculated[c]		1.4×10^{-8}	2.0×10^{-8}	1.0×10^{-8}	3.6×10^{-10}
Absolute Raman cross-section of $2\nu_{Au-Au}$ in $Å^2$/molecule					
$3\nu_{Au-Au}$	265	25	27	22	12

Table 2 (*Continued*)

Raman band	Raman shift (cm^{-1})[a]	Intensity[b]			
		252.7 nm	266.0 nm	273.9 nm	282.4 nm
$[Ag_2(dcpm)_2]^{2+}$ (**2**) (values from supporting information of [9])					
$-2\nu_{Ag-Ag}$	−163	–	3.5	3.4	2.9
$-\nu_{Ag-Ag}$	−80	41	63	55	61
ν_{Ag-Ag}	80	100	100	100	100
Experimental		1.02×10^{-8}	7.65×10^{-9}	3.64×10^{-9}	1.28×10^{-9}
Calculated[c]		9.54×10^{-9}	7.37×10^{-9}	4.09×10^{-9}	1.67×10^{-9}
Absolute Raman cross-section of ν_{Ag-Ag} in $Å^2$/molecule					
$2\nu_{Ag-Ag}$	163	32	25	32	20

Raman band	Raman shift (cm^{-1})[a]	Intensity[b]			
		282.4 nm	299.1 nm	309.1 nm	319.9 nm
$[Cu_2(dcpm)_2]^{2+}$ (**3**)					
$-2\nu_{Cu-Cu}$	−210	2	–	2	1.5
$-\nu_{Cu-Cu}$	−104	37	43	51	45
ν_{Cu-Cu}	104	100	100	100	100
Experimental		9.3×10^{-10}	5.9×10^{-9}	8.1×10^{-9}	4.9×10^{-9}
Calculated[c]		1.0×10^{-9}	6.1×10^{-9}	8.0×10^{-9}	5.4×10^{-9}
Absolute Raman cross-section of ν_{Cu-Cu} in $Å^2$/molecule					
$2\nu_{Cu-Cu}$	210	15	12	11	8

Raman band	Raman shift (cm^{-1})[a]	Intensity[b]			
		245.9 nm	252.7 nm	266.0 nm	273.9 nm
$Au_2(dmpm)_3(ClO_4)_2$ (**4**) (values from [11])					
$-2\nu_{Au-Au}$	−158	7	8	10	9
$-\nu_{Au-Au}$	−79	39	49	58	60
ν_{Au-Au}	79	100	100	100	100
Experimental		1.1×10^{-8}	1.7×10^{-8}	4.7×10^{-9}	9.9×10^{-10}
Calculated[c]		1.3×10^{-8}	2.7×10^{-8}	5.7×10^{-9}	9.9×10^{-10}
Absolute Raman cross-section of ν_{Au-Au} in $Å^2$/molecule					
$2\nu_{Au-Au}$	158	60	60	61	66
$3\nu_{Au-Au}$	237	18	12	9	10
$4\nu_{Au-Au}$	316	3	4	4	–

Raman band	Raman shift (cm^{-1})[a]	Intensity[b]			
		266.0 nm	273.9 nm	299.1 nm	319.9 nm
$Cu_2(dmpm)_3(ClO_4)_2$ (**5**)					
$-2\nu_{Au-Au}$	−150	–	10	8	5.5
$-\nu_{Au-Au}$	−75	46	48	50	42
ν_{Au-Au}	75	100	100	100	100
Experimental		4.0×10^{-9}	4.8×10^{-9}	2.9×10^{-10}	3.0×10^{-11}
Calculated[c]		4.5×10^{-9}	5.9×10^{-9}	1.8×10^{-10}	2.7×10^{-11}
Absolute Raman cross-section of ν_{Au-Au} in $Å^2$/molecule					
$2\nu_{Au-Au}$	150	55	53	58	62

[a] Estimated uncertainties are about 4 cm^{-1} for the Raman shifts.

[b] Relative intensities are based on integrated areas of Raman bands. Estimated uncertainties are about 5% for intensities greater than 100, 10% for intensities between 50 and 100, and 20% for intensities below 50.

[c] Calculated using the parameters of this table in Eqs. (1) and (2) and the overdamped Brownian oscillator damping function for solvent dephasing.

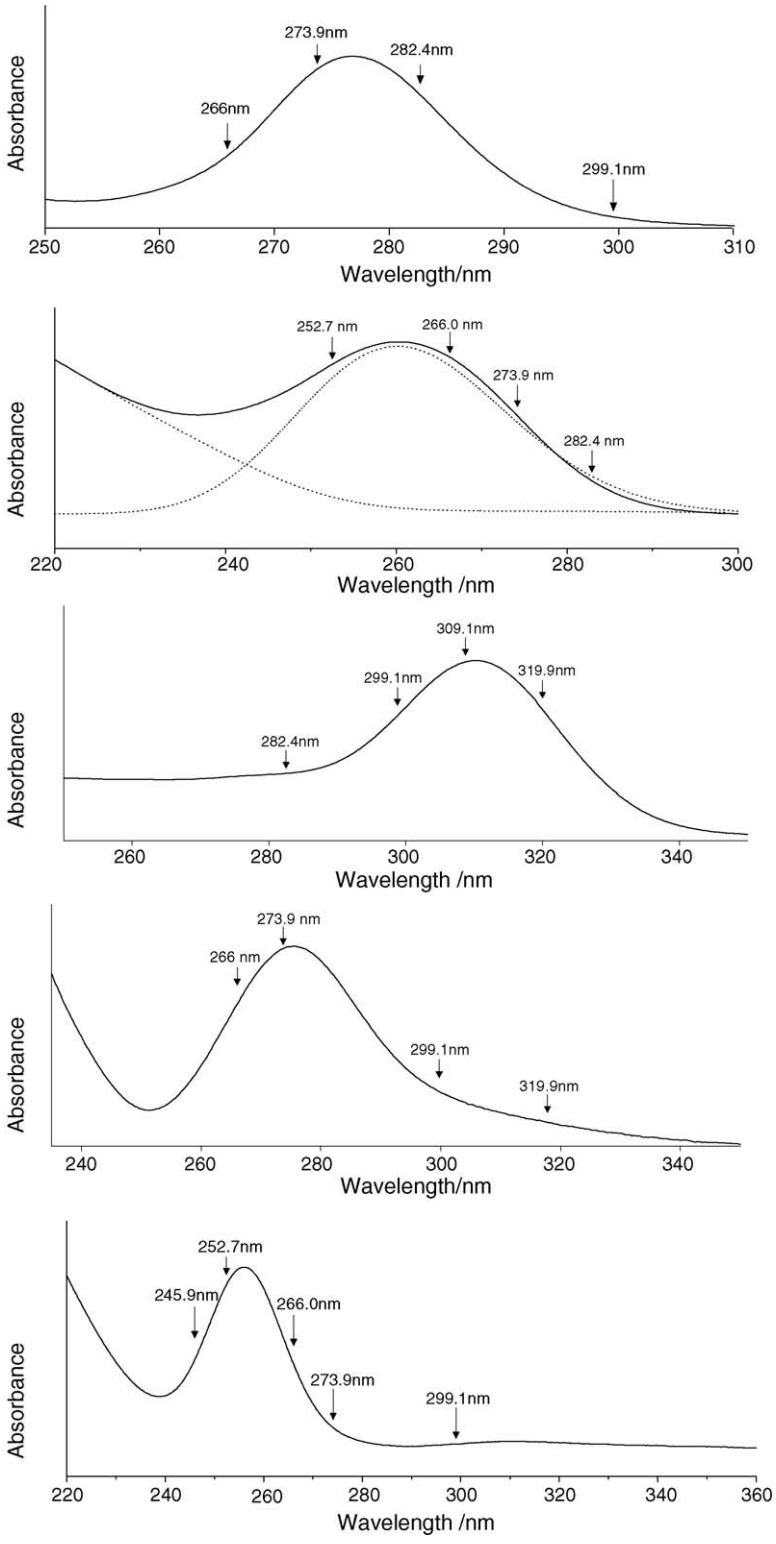

Fig. 3. Absorption spectra of $[Au_2(dcpm)_2]^{2+}$ (**1**) and $[Ag_2(dcpm)_2]^{2+}$ (**2**) in acetonitrile solution, $[Cu_2(dcpm)_2]^{2+}$ (**3**) in dichloromethane solution, and $[Au_2(dmpm)_3]^{2+}$ (**4**) and $[Cu_2(dmpm)_3]^{2+}$ (**5**) in water solution at room temperature with the excitation wavelengths for the resonance Raman experiments indicated above the spectra.

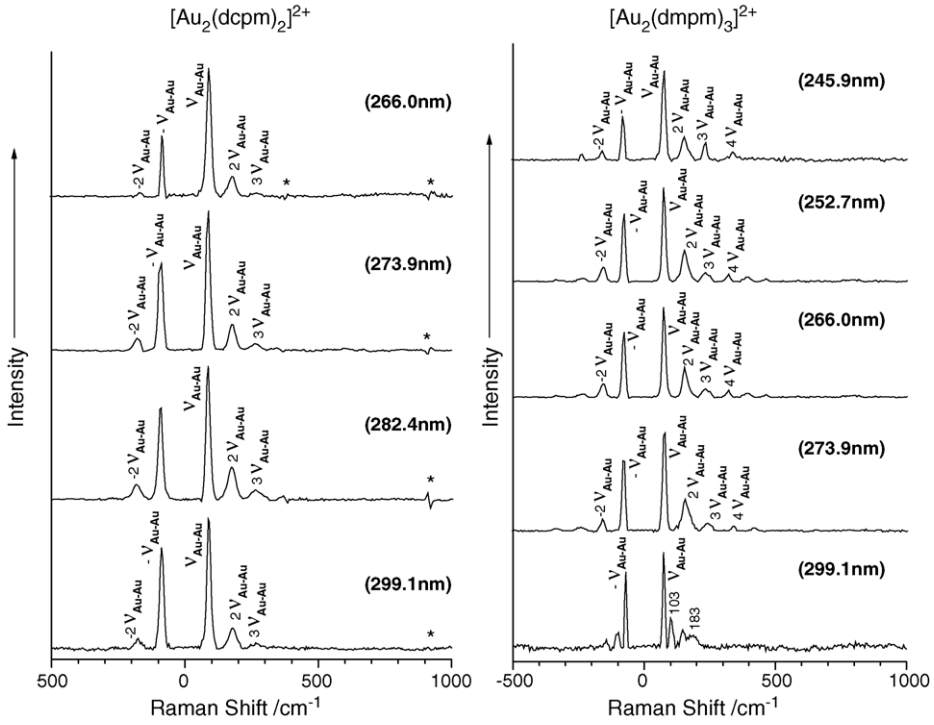

Fig. 4. Overview of the resonance Raman spectra of **1** (in acetonitrile solution obtained with 266.0, 273.9, 282.4, and 299.1 nm excitation) and **4** (in water solution obtained with 245.9, 252.7, 266.0, and 273.9 nm excitation). The spectra have been intensity corrected and the Rayleigh line, glass bands and solvent bands have been subtracted. The Raman band assignments are shown next to the bands and asterisks mark regions were solvent subtraction artifacts are present. The spectra for **1** and **4** are from [8,11], respectively.

compared to their ground electronic state vibrational frequencies (see Table 4). This is consistent with the proposed ndσ* → (n + 1)pσ absorption band assignment for the transitions ∼277 nm for **1**, ∼260 nm for **2**, and ∼310 nm for **3**, ∼256 nm for **4**, ∼276 nm for **5**. The Au–Au stretching excited state frequency for **1** (estimated to be 175 cm^{-1}) is similar to the related Pt–Pt stretching frequency of 156 cm^{-1} in the ^{3}[dσ*pσ] excited state of $[Pt_2(P_2O_5H_2)_4]^{4+}$ which is considered to have a single metal–metal bond [38,39] and this accords well with the ^{1}[dσ*pσ] excited states visualized to have close to a bond order of one.

Examination of the best-fit parameters of Table 3 shows that a noticeable amount of inhomogeneous broadening is needed in order to simultaneously simulate the absolute resonance Raman cross-sections and absorption bandwidth. The source of this inhomogeneous broadening is probably weak interaction of the cation with solvent and/or anion yielding species with moderately different transition energies for the ^{1}[dσ*pσ] state. A small cation–anion interaction in the ground state of $[Au_2(dcpm)_2](ClO_4)_2$ was found in the X-ray crystal structure with the Au atom having a T-shaped geometry and average Au···O(ClO_4) distances of 3.36(2) Å [13,14]. Similarly, both the crystal structures of $[Ag_2(dcpm)_2](SO_3CF_3)_2$ and $[Cu_2(dcpm)_2](ClO_4)_2$ reveal the existence of ground state cation–anion interactions ($d_{Ag–O(SO_3CF_3)}$ = 2.692(7) Å in **2** [9] and $d_{Cu–O(ClO_4)}$ = 2.687(av) Å in **3** [10]), that are apparently stronger than that in $[Au_2(dcpm)_2](ClO_4)_2$. Ab initio calculations [7] indicated that the model compound $[Au_2(H_2PCH_2PH_2)_2]^{2+}$ interacts with acetonitrile molecules weakly in the ground electronic state but strongly in the excited electronic states. These calculations showed that structures of the uncomplexed $Au_2(H_2PCH_2PH_2)_2{}^{2+}$ and the $\{Au_2(H_2PCH_2PH_2)_2{\cdot}(MeCN)_2\}^{2+}$ complex have very similar Au–Au distances in the $^1A_{1g}$ ground electronic state (3.167 and 3.155 Å, respectively) [7]. The ^3A_u state (^{3}[dσ*pσ]) of $\{Au_2(H_2PCH_2PH_2)_2{\cdot}(MeCN)_2\}^{2+}$ was computed to have a much shorter equilibrium Au–Au distance (∼2.719 Å) [7]. The resonance Raman intensity analysis given here for the ndσ* → (n + 1)pσ transitions of **1** and **2** in acetonitrile and **3** in dichloromethane refers to unrelaxed excited states for which strong exciplexes with solvent could be produced by the time-scale, but weak solvent/anion interactions with the ground state may contribute to the inhomogeneous broadening, particularly because of serendipitous ground state solvent/anion configurations that correspond to exciplex geometry (in an angular sense rather than in bond lengths) could result in substantially shifted electronic energies. Further work is needed to confirm this and a time-resolved resonance Raman (TR^3) study of the ^{1}[dσ*pσ] and/or ^{3}[dσ*pσ] states could directly probe the uncomplexed and complexed forms of the compounds and possibly reveal

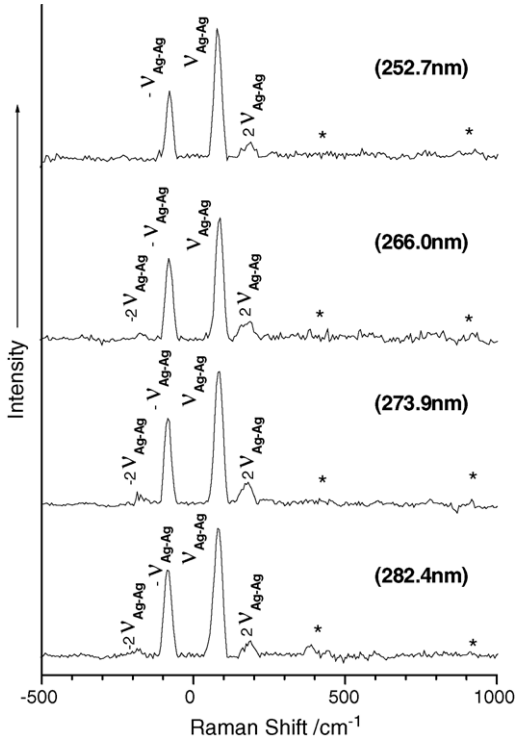

Fig. 5. Overview of the resonance Raman spectra of **2** in acetonitrile solution obtained with 252.7, 266.0, 273.9, and 282.4 nm excitation wavelengths. The spectra have been intensity corrected and the Rayleigh line, glass bands and solvent bands have been subtracted. Asterisks mark regions were solvent subtraction artifacts are present and the Raman band assignments are shown next to the bands. The 273.9 nm spectrum is from [9].

the extent of the solvent interaction in these electronic excited states.

*4.3. Comparison of the force constants and metal–metal separations for the ground electronic state and the excited $^1[d\sigma^*p\sigma]$ electronic state for dibridged $[M_2(dcpm)_2]^{2+}$ (M = Au, **1**; Ag, **2**; Cu, **3**) and tribridged $[M_2(dmpm)_3]^{2+}$ (M = Au, **4**; Cu, **5**) compounds with those for other Au, Ag, and Cu dimer compounds*

It is interesting to compare the force constants and metal–metal separations for the ground electronic state and the excited $^1[d\sigma^*p\sigma]$ electronic state for **1**–**5** with those for other Au, Ag, and Cu dimer compounds [40–43]. Tables 5 and 6 compare the Au–Au and Ag–Ag stretch frequencies, force constants and bond lengths for **1**, **2**, and **4** with other compounds [40–42]. Harvey and co-workers [40,41,44] found a good linear correlation for the Au–Au bond distance versus ln *F*(Au–Au) for 11 compounds and the Ag–Ag bond distance versus ln *F*(Ag–Ag) for 9 compounds. These workers determined empirical relationships given by the following formulas:

$$r(\text{Au–Au}) = -0.290 \ln F(\text{Au–Au}) + 2.68 \quad (5)$$

Table 3
Parameters for simulations of resonance Raman intensities and absorption spectra of $[Au_2(dcpm)_2]^{2+}$ (**1**) in acetonitrile solution, $[Ag_2(dcpm)_2]^{2+}$ (**2**) in acetonitrile solution and $[Cu_2(dcpm)_2]^{2+}$ (**3**) in dichloromethane solution

Ground state vibrational frequency (cm^{-1})	Excited state vibrational frequency (cm^{-1})	Δ
$Au_2(dcpm)_2(ClO_4)_2$ (**1**) (values from [8])		
88	175	0.68
E_0 = 34,000 cm^{-1}, M = 0.995 Å, n = 1.344		
Homogeneous broadening, Γ = 2150 cm^{-1} FWHM		
Inhomogeneous broadening, G = 200 cm^{-1} standard deviation		
Brownian oscillator Λ = 55.3 cm^{-1}, D = 2048 cm^{-1}		
$[Ag_2(dcpm)_2]^{2+}$ (**2**) (values from supporting information of [9])		
80	180	0.90
E_0 = 31,000 cm^{-1}, M = 0.91 Å, n = 1.344		
Homogeneous broadening, Γ = 4050 cm^{-1} FWHM		
Inhomogeneous broadening, G = 100 cm^{-1} standard deviation		
Brownian oscillator Λ = 17.2 cm^{-1}, D = 7156 cm^{-1}		
$[Cu_2(dcpm)_2]^{2+}$ (**3**)		
104	150	1.10
E_0 = 28,950 cm^{-1}, M = 0.895 Å, n = 1.426		
Homogeneous broadening, Γ = 2700 cm^{-1} FWHM		
Inhomogeneous broadening, G = 300 cm^{-1} standard deviation		
Brownian oscillator Λ = 81.1 cm^{-1}, D = 3243 cm^{-1}		
$[Au_2(dmpm)_3]^{2+}$ (**4**) (values from [11])		
79	165	0.65
E_0 = 35,600 cm^{-1}, M = 0.895 Å, n = 1.36		
Homogeneous broadening, Γ = 2750 cm^{-1} FWHM		
Inhomogeneous broadening, G = 250 cm^{-1} standard deviation		
Brownian oscillator Λ = 11.69 cm^{-1}, D = 3,299 cm^{-1}		
$[Cu_2(dmpm)_3]^{2+}$ (**5**)		
75	168	0.665
E_0 = 31,210 cm^{-1}, M = 0.772 Å, n = 1.36		
Homogeneous broadening, Γ = 3330 cm^{-1} FWHM		
Inhomogeneous broadening, G = 500 cm^{-1} standard deviation		
Brownian oscillator Λ = 14.16 cm^{-1}, D = 4838 cm^{-1}		

Note: M = transition length, n = index of refraction, and Δ = normal mode displacement of the excited state relative to the ground electronic state.

$$r(\text{Ag–Ag}) = -0.284 \ln F(\text{Ag–Ag}) + 2.53 \quad (6)$$

where r(Au–Au) and r(Ag–Ag) are Au–Au and Ag–Ag bond distances (in Å), respectively; F(Au–Au) is the force constant of the Au–Au bond and F(Ag–Ag) is the force constant of the Ag–Ag bond (in mdyne/Å). There has been no reported correlation for Cu_2 bonds, thus we used an alternative bond

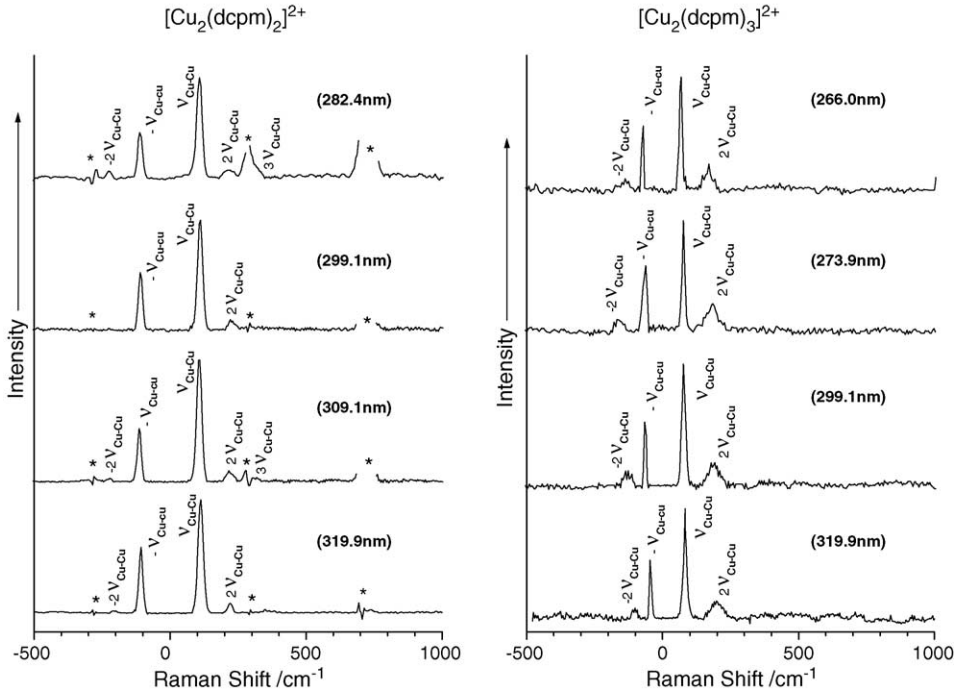

Fig. 6. Overview of the resonance Raman spectra of **3** (in dichloromethane solution obtained with 282.4, 299.1, 309.1, and 319.9 nm excitation) and **5** (in water solution with 266.0, 273.9, 299.1, and 319.9 nm excitation). The spectra have been intensity corrected and the Rayleigh line, glass bands and solvent bands have been subtracted. Asterisks mark regions were solvent subtraction artifacts are present and the Raman band assignments are shown next to the bands. The 299.1 nm spectrum of **3** is from [10].

length/force constant correlation given by Woodruff and coworkers [42]. Woodruff's equations are fits to combined data for given rows of the periodic table; thus, his equations for Cu_2, Ag_2, and Au_2 bonds are actually a general correlation for a particular row of the periodic table, respectively. Woodruff's broad correlations perform somewhat more poorly for the Ag_2 and Au_2 cases than Harvey's element-specific ones and we do not present these correlations here. Woodruff's third row correlation, Eq. (7), is however, the only one available for Cu_2 bonds at this time (Table 7):

$$r(3\text{-}3) = 1.81 + 1.22 \exp\left(\frac{-F}{2.37}\right) \quad (7)$$

Figs. 10–12 show plots of the M–M bond distance versus $\ln F$(M–M) for the correlation functions in Eqs. (5)–(7) (where M = Au or Ag or Cu) and the data presented in Tables 5 and 6 for the ground and excited states of **1**–**5** and the other compounds. Inspection of Fig. 10 shows that the 11 compounds and the ground state of **1** and **4** have Au–Au bond distances and $\ln F$(Au–Au) values close to the "Au–Au" correlation curve (Eq. (5)) [44]. Similarly, inspection of Fig. 11 reveals the nine compounds and the ground state of **2** have Ag–Ag bond distances and ln F(Ag–Ag) values close to the "Ag–Ag" correlation curve (Eq. (6)) [40]. However, the ^{1}[dσ*pσ] excited state of **1**, **2**, and **4** values are significantly farther from the correlation curves and

Table 4
Ground and excited state vibrational frequencies, normal mode displacements and change in metal–metal bond length in excited state relative to ground state for **1**–**5**

Compound	Ground state vibrational frequency (cm^{-1})	Ground state M–M distance (Å)	Excited state vibrational frequency (cm^{-1})[a]	$\|\Delta\|$[a]	ΔM–M bond in excited state (Å)[b]
$[Au_2(dcpm)_2]^{2+}$ (**1**)	88	2.9153[c]	175	0.68	0.11
$[Ag_2(dcpm)_2]^{2+}$ (**2**)	80	2.960[d]	180	0.90	0.20
$[Cu_2(dcpm)_2]^{2+}$ (**3**)	104	2.730[c]	150	1.10	0.28
$[Au_2(dmpm)_3]^{2+}$ (**4**)	79	3.028[c]	165	0.65	0.11
$[Cu_2(dmpm)_3]^{2+}$ (**5**)	75	3.021[c]	168	0.665	0.20

[a] Values from best-fit parameters of Table 2.
[b] Values determined using the parameters of Table 2 in Eq. (4).
[c] For ClO_4 salt.
[d] For CF_3SO_3 salt.

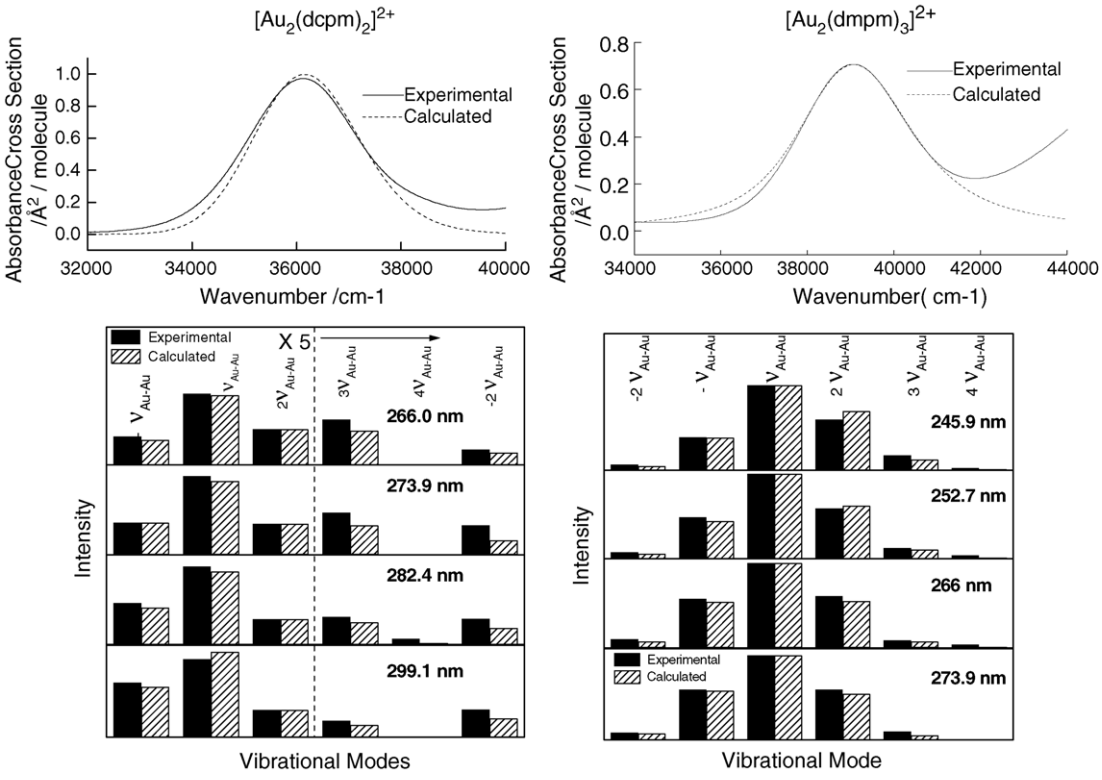

Fig. 7. (Top) Comparison of the calculated (dashed line) and experimental (solid line) absorption spectra for **1** in acetonitrile solution (left: from [8]) and for **4** in water solution (right: from [11]). (Bottom) Comparison of the calculated (dashed bar) and experimental (solid bar) resonance Raman intensities for these resonance Raman spectra of **1** and **4** are shown in Fig. 3. The parameters given in Table 2 for **1** and **4** were used in Eqs. (1) and (2) to calculate the absorption and resonance Raman intensities (the model described in Section 3 and an overdamped Brownian oscillator solvent dephasing function were used for these calculations).

Table 5
Structural and spectroscopic data for selected Au_2 compounds

Compound[a]	ν(Au–Au) (cm^{-1})	F(Au–Au) (mdyne/Å)	ln F(Au–Au)	r(Au–Au) (Å)
$Au_2(dmb)(CN)_2$	36	0.075	−2.59	3.536
$Au_2(tmb)Cl_2$	50	0.14	−1.97	3.301
$Au_2(ylide)_2$	64	0.24	−1.43	2.977
$[Au_2(dmpm)_3](PF_6)_2$	68	0.27	−1.31	3.045
$[Au_2(dmpm)_2](PF_6)_2$	69	0.28	−1.27	3.044
$[Au_2(dmpm)_2]Cl_2$	71	0.29	−1.24	3.010
$Au_2(ylide)_2Cl_2$	162	1.98	0.68	2.597
$Au_2^+(^2\Sigma_u^+)$	149	1.29	0.25	2.582
$Au_2(^3\Sigma_u^+)$	142	1.18	0.165	2.568
$Au_2(^1\Sigma_g^+)$	180	1.88	0.63	2.520
$Au_2(^1\Sigma_u^+)$	191	2.11	0.75	2.472
$[Au_2(dcpm)_2]^{2+}$ (**1**)	88	0.449	−0.80	2.92[b]
$[Au_2(dcpm)_2]^{2+}$ (**1**), excited state $^1[d\sigma^*p\sigma]$	175[c]	1.777	0.57	2.81[c]
	145[d]	1.220	0.20	2.81[c]
$[Au_2(dmpm)_3]^{2+}$ (**4**)	79	0.362	−1.016	3.028[b]
$[Au_2(dmpm)_3]^{2+}$ (**4**), excited state $^1[d\sigma^*p\sigma]$	165[c]	1.580	0.46	2.921[c]

[a] The values for the first 11 compounds of this table come from Table VIII of [40] which also lists the original references from which these values can be found.
[b] Value from [13,14] for ClO_4 salt.
[c] Values from resonance Raman intensity analysis of this work.
[d] Possible value if resonance Raman intensity analysis overestimates excited state frequency (see text).

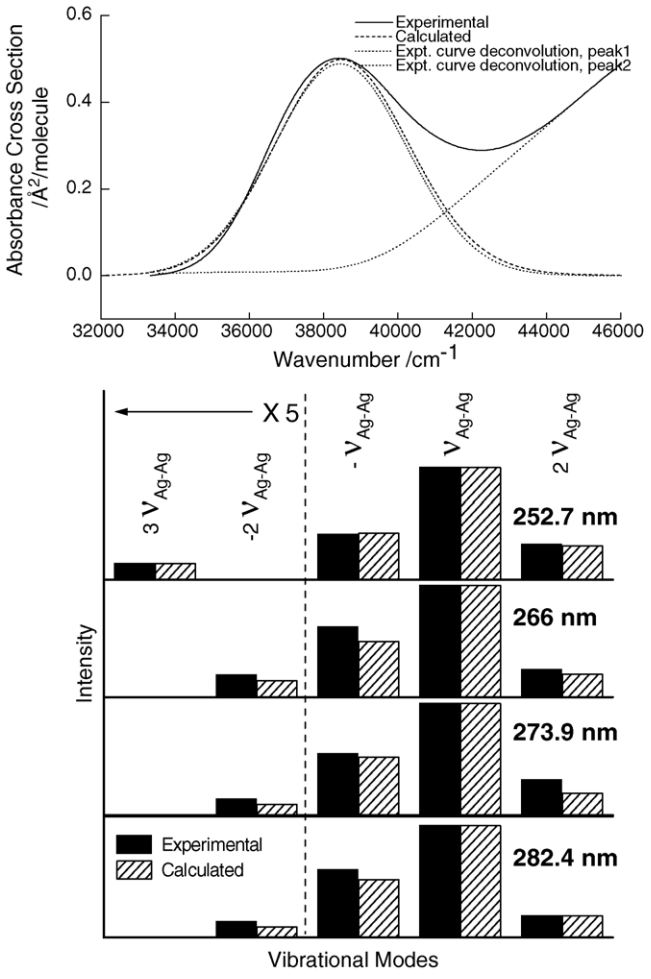

Fig. 8. (Top) Comparison of the calculated (dashed line) and experimental (solid line) absorption spectra for **2** in acetonitrile solution. (Bottom) Comparison of the calculated (dashed bar) and experimental (solid bar) resonance Raman intensities for the 252.7, 266.0, 273.9, and 282.4 nm resonance Raman spectra. The parameters given in Table 2 for **2** were used in Eqs. (1) and (2) to calculate the absorption and resonance Raman intensities (the model described in Section 3 and an overdamped Brownian oscillator solvent dephasing function were used for these calculations).

this could be due to several possibilities. First, we may be overestimating the excited state frequency. Our previous study for the $5d\sigma^* \rightarrow 6p\sigma$ transition of $[Pt_2(P_2O_5H_2)_4]^{4-}$ showed that the $^1[d\sigma^*p\sigma]$ excited state frequency determined from the resonance Raman intensity analysis was about 177 cm^{-1} [19] compared to ~146 cm^{-1} from the low temperature absorption spectra [6,43]. However, both the resonance Raman intensity analysis and a Franck–Condon analysis of the low temperature absorption spectra gave almost the same excited state Pt–Pt bond length change (~0.225 and 0.21 Å) [6,19,43]. Thus, the excited state frequencies derived from the resonance Raman intensity analysis may be somewhat too high due to neglecting the change of the transition length as a function of bond length and/or anharmonicity. If our analysis for compounds **1** and **2**, for example, have a similar over estimation of the excited state frequency (say 30 cm^{-1} from 175 to 145 cm^{-1} in the case of **1** or from 180 to 150 cm^{-1} for **2**) then the $\ln F$(Au–Au) and $\ln F$(Ag–Ag) values shift noticeably toward the correlation curve (see open circle points in Figs. 10 and 11). However, the agreement is still not very good. This suggests that some overestimation of the excited state vibrational frequencies by the resonance Raman intensity analysis cannot fully account for the differences between the excited states of **1** and **2** and the correlation curves shown in Figs. 10 and 11.

We note that the different electronic states of the Au_2 dimer can show noticeable variation in the vibrational frequency (from 142 cm^{-1} for $Au_2(^3\Sigma_u^+)$ to 191 cm^{-1} for $Au_2(^1\Sigma_u^+)$) and the $Au_2(ylide)_2Cl_2$ compound is also somewhat far from the Au correlation curve. There is also noticeable variation in the $Ag_2(dmb)X_2$ values (where X = Cl, Br or I). Thus, a second possibility to be considered is that the excited states of **1**, **2**, and **4** do not follow the "Au–Au" and "Ag–Ag" correlation curves very well (and likely **3** and **5** for the Woodruff third row correlation) due to solvent interactions in the initially excited state. This has been described in a previous section and in recent ab initio work on a model compound similar to **1** and experimental photoluminescence work on **1** [7]. These solvent–solute interactions of the $[d\sigma^*p\sigma]$ excited states would likely perturb the metal–metal bond length and force constant so that the metal–metal bond length versus $\ln F$(M–M) correlation for these excited states could be significantly different than one would obtain for similar metal–metal interactions which do not strongly interact with the solvent. As revealed by UV–vis absorption spectroscopy, the ground states of **1**, **2**, and **4** show little if any interaction with the solvent used for resonance Raman experiments with very small perturbation of the ground state metal–metal bond lengths. Thus, the ground states of **1**, **2**, and **4** follow the "Au–Au" and "Ag–Ag" correlation well (see Figs. 10 and 11). However, the initially formed $^1[d\sigma^*p\sigma]$ excited states of **1**, **2**, and **4** exhibit strong differences with the "Au–Au" and "Ag–Ag" correlation curves. In addition, the trends found for the metal–metal bond lengths and force constants as the metal dimer is varied from Au to Ag to Cu does not follow the expected pattern. This could be due to the peculiarities in the solvent–solute interaction for each of the compounds (**1**–**5**). Compound **3** exhibits significantly ground state solvent–solute interaction than **1** and **2**. The interaction of coordinating solvent such as CH_3CN with the $[Cu_2(dcpm)_2]^{2+}$ core has also been confirmed by UV–vis absorption spectroscopy—the $^1[d\sigma^*p\sigma]$ absorption band of **3** recorded in CH_2Cl_2 becomes less distinct in CH_3CN, on the other hand, the absorption spectra of **1** and **2** are similar in both CH_2Cl_2 and CH_3CN solutions. Thus, it would not be too surprising that the excited state solvent–solute interactions strongly depend on the metal as well to noticeably perturb the expected pattern of the bond lengths and force constants as the metal is varied from Au to Cu. We also note the recent observation of bond stretch isomerism coupled to ligand

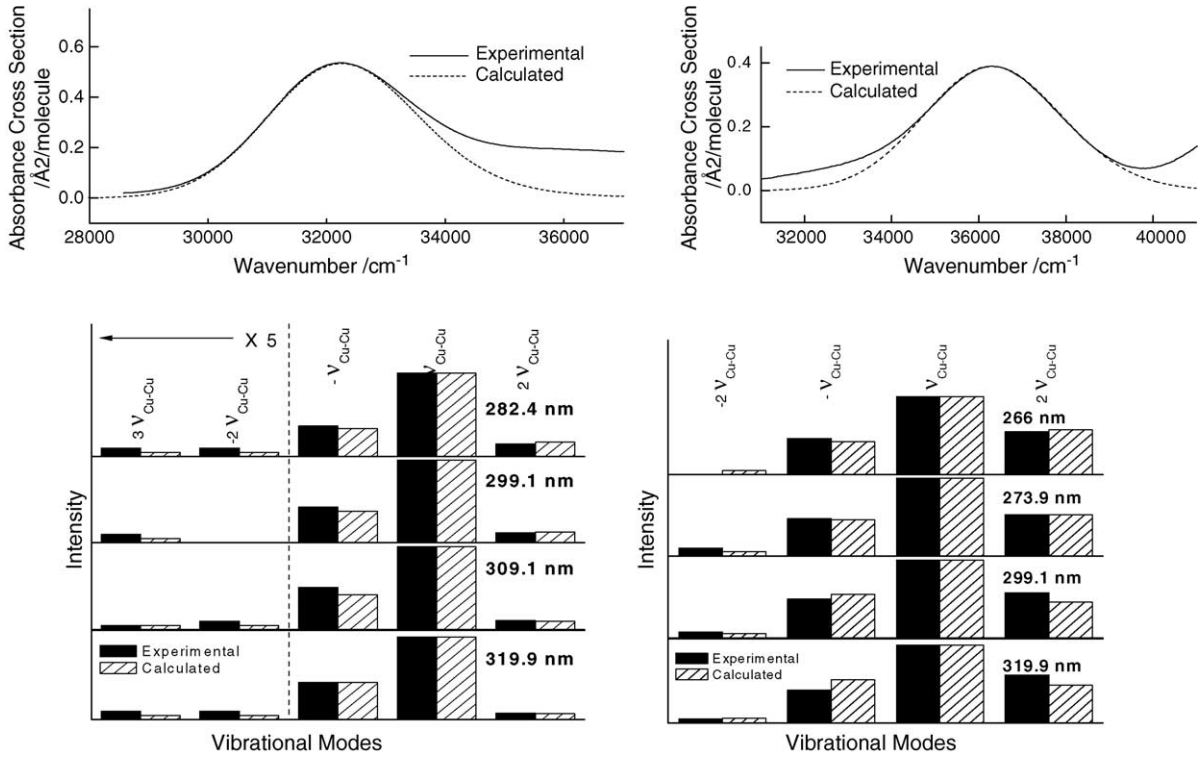

Fig. 9. (Top) Comparison of the calculated (dashed line) and experimental (solid line) absorption spectra for **3** in dichloromethane solution (left) and for **5** in water solution (right). (Bottom) Comparison of the calculated (dashed bar) and experimental (solid bar) resonance Raman intensities for the resonance Raman spectra of **3** and **5** shown in Fig. 5. The parameters given in Table 2 for **3** and **5** were used in Eqs. (1) and (2) to calculate the absorption and resonance Raman intensities (the model described in Section 3 and an overdamped Brownian oscillator solvent dephasing function were used for these calculations).

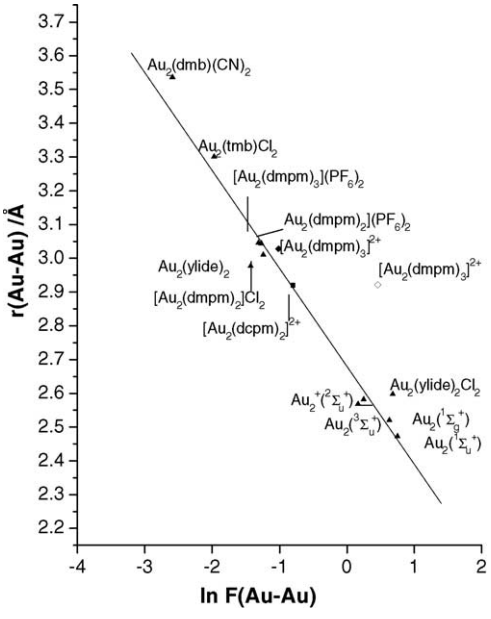

Fig. 10. Plot of r(Au–Au) vs. ln F(Au–Au) for the 11 compounds (closed triangles), the ground (closed square) and excited state (closed circle) of **1** and the ground (closed diamond) and excited state (open diamond) of **4** given in Table 4 (a similar comparison for dinuclear Au complexes was made in the supporting information of [11]). The line shows the "Au–Au" correlation curve (Eq. (5)). The open circle shows the effect of lowering the excited state vibrational frequency of **1** by 30 cm^{-1} (see text).

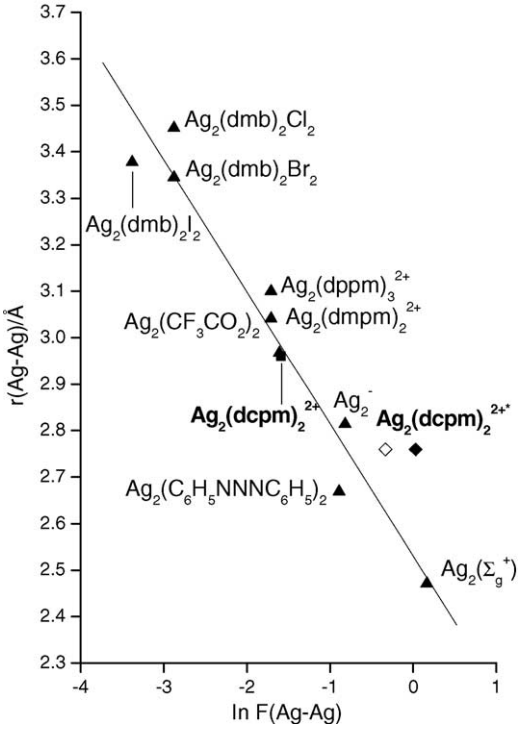

Fig. 11. Plot of r(Ag–Ag) vs. ln F(Ag–Ag) for the 11 compounds (closed triangles) and the ground (closed square) and excited state (closed circle) of **2** given in Table 5. The line shows the "Ag–Ag" correlation curve (Eq. (6)). The open circle shows the effect of lowering the excited state vibrational frequency of **2** by 30 cm^{-1} (see text).

Table 6
Structural and spectroscopic data for selected Ag_2 compounds

Compound[a]	ν(Ag–Ag) (cm^{-1})	F(Ag–Ag) (mdyne/Å)	ln F(Ag–Ag)	r(Ag–Ag) (Å)
$Ag_2(dmb)_2I_2$	33	0.034	−3.38	3.378
$Ag_2(dmb)_2Cl_2$	42	0.056	−2.88	3.451
$Ag_2(dmb)_2Br_2$	42	0.056	−2.88	3.345
$[Ag_2(dmpm)_3](PF_6)_2$	76	0.18	−1.71	3.10[b]
$[Ag_2(dmpm)_2](PF_6)_2$	76	0.18	−1.71	3.041
$Ag_2(O_2CCF_3)_2$	80	0.20	−1.61	2.967
$Ag_2(C_6H_5NNNC_6H_5)_2$	114	0.41	−0.89	2.669
$Ag_2^-(^2\Sigma_u^+)$	118	0.44	−0.82	2.814
$Ag_2(^1\Sigma_g^+)$	192.8	1.18	0.1655	2.471
$[Ag_2(dcpm)_2]^{2+}$ (**2**)	80	0.203	−1.59	2.96[c]
$[Ag_2(dcpm)_2]^{2+}$ (**2**), excited state $^1[d\sigma^*p\sigma]$	180[d]	1.029	0.028	2.76[d]
	150[e]	0.715	−0.335	2.76[d]

[a] The values for the first nine compounds of this table come from Table VIII of [41] which also lists the original references from which these values can be found.
[b] Value from [12].
[c] Value from [9] for CF_3SO_3 salt.
[d] Values from resonance Raman intensity analysis of this work and supporting information of [9].
[e] Possible value if resonance Raman intensity analysis overestimates excited state frequency (see text).

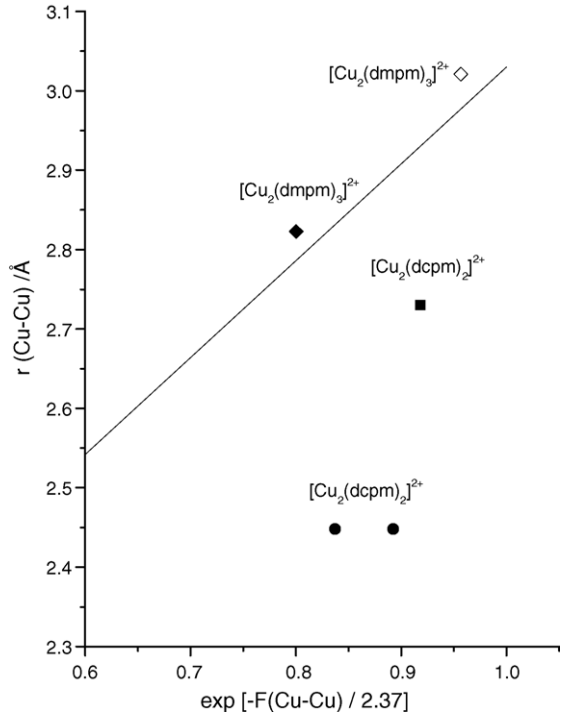

Fig. 12. Plot of r(3-3) vs. exp(−F(3-3)/2.37) for the ground (closed square) and excited state (closed circle) of **3** and ground (closed diamond) and excited state (open diamond) of **5** given in Table 6. The line shows the "Woodruff" correlation curve (Eq. (7)). The open circle shows the effect of lowering the excited state vibrational frequency of **3** by 30 cm^{-1} (see text).

deformation (or distortional isomerism) reported for a mixed valence Cu dimer complex [45]. The X-ray crystal structure of $[Cu_2(dcpm)_2]X_2$ (X = anion) also reveals close Cu(I)–anion interaction.

Table 7
Structural and spectroscopic data for selected Cu_2 compounds

Compound[a]	ν(Cu–Cu) (cm^{-1})	F(Cu–Cu) (mdyne/Å)	r(Cu–Cu) (Å)
$[Cu_2(dcpm)_2]^{2+}$ (**3**)	104	0.2025	2.730[a]
$[Cu_2(dcpm)_2]^{2+}$ (**3**), excited state $^1[d\sigma^*p\sigma]$	150	0.4212	2.448[b]
	120[c]	0.2696	2.448[b]
$[Cu_2(dmpm)_3]^{2+}$ (**5**)	75	0.1053	3.021[a]
$[Cu_2(dmpm)_3]^{2+}$ (**5**), excited state $^1[d\sigma^*p\sigma]$	168	0.5283	2.823[b]

[a] Value from [10,12] for ClO_4 salt.
[b] Values from resonance Raman intensity analysis of this work.
[c] Possible value if resonance Raman intensity analysis overestimates excited state frequency (see text).

5. Concluding remarks and future prospects

The UV–vis and resonance Raman spectroscopic investigation of the lowest energy dipole-allowed absorption band of $[M_2(dcpm)_2]^{2+}$ (M = Au, Ag, Cu) and $[M_2(dmpm)_3]^{2+}$ (M = Au, Ag, Cu) complexes was detailed. The UV–vis absorption spectra of $[M_2(dcpm)_2]^{2+}$ and $[M_2(dmpm)_3]^{2+}$ exhibit an intense low energy $nd\sigma^* \rightarrow (n+1)p\sigma$ transition with its transition energy increasing as one goes from two- to three-coordinated complexes. The transition energy for the $[M_2(dcpm)_2]^{2+}$ complexes follows the order: Ag > Au > Cu. A resonance Raman intensity analysis of the spectra was done to extract an estimate of the structural changes of the $^1[d\sigma^*p\sigma]$ excited states relative to the ground state. The structural changes in these compounds were compared with each other and with other related compounds. The metal–metal bonds were observed to be very similar for the ground and excited states of the $[Au_2(dcpm)_2]^{2+}$ and

$[Au_2(dmpm)_3]^{2+}$ complexes but significantly different for the $[Cu_2(dcpm)_2]^{2+}$ and $[Cu_2(dmpm)_3]^{2+}$ complexes that exhibit weaker metal–metal bonding. The ground states of **1**, **2**, and **4** were found to follow the "Au–Au" and "Ag–Ag" correlation well (see Figs. 10 and 11). However, the initially formed $^1[d\sigma^*p\sigma]$ excited states of **1**, **2**, and **4** exhibit strong differences with the "Au–Au" and "Ag–Ag" correlation curves. This is probably due to solvent interactions in the initially excited state and some indirect evidence for this was discussed.

We have recently begun to explore for potential metal–metal interactions in other binuclear metal complexes containing Ni and Pt [46] and mixed d^8–d^{10} binuclear complexes containing Pt and Au or Pt and Cu [47]. In addition, it would be interesting to extend these UV–vis and resonance Raman studies to trinuclear and larger organometallic complexes to try and better understand their specific metal–metal interactions in both their ground and excited states. In particular, time-resolved studies like time-resolved resonance Raman spectroscopy [48] would be very useful to directly investigate the excited state metal–metal bonding and its interaction with solvent and/or substrates and possible exciplex formation. Further work on characterizing weak metal–metal interactions in binuclear and other coordination compounds appears very promising and a range of experimental and theoretical methods can be employed to investigate these species to learn even more details in the future.

Acknowledgments

Grants from the Committee on Research and Conference Grants (CRCG), the Research Grants Council (RGC) of Hong Kong and the Large Items of Equipment Allocation 1993–1994 and 2000–2001 from the University of Hong Kong supported this work.

References

[1] J.V. Caspar, J. Am. Chem. Soc. 107 (1985) 6718.
[2] P.D. Harvey, H.B. Gray, J. Am. Chem. Soc. 110 (1988) 2145.
[3] C.-M. Che, H.L. Kwong, V.W.W. Yam, K.C. Cho, J. Chem. Soc., Chem. Commun. (1989) 885.
[4] C. King, J.-C. Wang, Md.N.I. Khan, J.P. Fackler Jr., Inorg. Chem. 28 (1989) 2145.
[5] K.R. Mann, J.G. Gordon II, H.B. Gray, J. Am. Chem. Soc. 97 (1975) 3553.
[6] S.F. Rice, H.B. Gray, J. Am. Chem. Soc. 105 (1983) 4571.
[7] H.Z. Zhang, C.-M. Che, Chem. Eur. J. (2001) 4887.
[8] K.H. Leung, D.L. Phillips, M.-C. Tse, C.M. Che, V.M. Miskowski, J. Am. Chem. Soc. 121 (1999) 4799.
[9] C.-M. Che, M.-C. Tse, M.C.-W. Chan, K.K. Cheung, D.L. Phillips, K.H. Leung, J. Am. Chem. Soc. 122 (2000) 2464.
[10] C.-M. Che, Z. Mao, V.M. Miskowski, M.-C. Tse, C.-K. Chan, K.K. Cheung, D.L. Phillips, K.H. Leung, Angew. Chem. 39 (2000) 4084.
[11] K.H. Leung, D.L. Phillips, Z. Mao, C.-M. Che, V.M. Miskowski, C.K. Chan, Inorg. Chem. 41 (2002) 2054.
[12] D. Li, C.-M. Che, H.L. Kwong, V.W.W. Yam, J. Chem. Soc., Dalton Trans. (2002) 3325.
[13] W.F. Fu, K.C. Chan, K.K. Cheung, V.M. Miskowski, C.-M. Che, Angew. Chem. Int. Ed. Engl. 38 (1999) 2783.
[14] W.F. Fu, K.C. Chan, K.K. Cheung, C.-M. Che, Chem. Eur. J. 7 (2001) 4656.
[15] C.K. Chan, Ph.D. thesis, The University of Hong Kong, 1997.
[16] W.M. Kwok, D.L. Phillips, P.K.-Y. Yeung, V.W.W. Yam, Chem. Phys. Lett. 262 (1996) 699.
[17] W.M. Kwok, D.L. Phillips, P.K.-Y. Yeung, V.W.W. Yam, J. Phys. Chem. A 101 (1997) 9286.
[18] X. Zheng, D.L. Phillips, J. Chem. Phys. 110 (1999) 1638.
[19] K.H. Leung, D.L. Phillips, C.-M. Che, V.M. Miskowski, J. Raman Spectrosc. 30 (1999) 987.
[20] E.C.-C. Cheng, K.-H. Leung, V.M. Miskowski, V.W.W. Yam, D.L. Phillips, Inorg. Chem. 39 (2000) 3690.
[21] A.B. Myers, B. Li, X. Ci, J. Chem. Phys. 89 (1988) 1876.
[22] M.O. Trulson, R.A. Mathies, J. Chem. Phys. 84 (1986) 2068.
[23] J.M. Dudik, C.R. Johnson, S.A. Asher, J. Chem. Phys. 82 (1985) 1732.
[24] A.B. Myers, Laser Techniques in Chemistry, Wiley, New York, 1995, p. 325.
[25] S.Y. Lee, E.J. Heller, J. Chem. Phys. 71 (1979) 4777.
[26] A.B. Myers, R.A. Mathies, D.J. Tannor, E.J. Heller, J. Chem. Phys. 77 (1982) 3857.
[27] L. Tutt, D. Tannor, E.J. Heller, J.I. Zink, Inorg. Chem. 21 (1982) 3858.
[28] A.B. Myers, R.A. Mathies, Biological Applications of Raman Spectroscopy, Wiley, New York, 1987, p. 1.
[29] R.J.H. Clark, T.J. Dines, Angew. Chem. Int. Ed. Engl. 98 (1986) 131.
[30] S.K. Doorn, J.T. Hupp, J. Am. Chem. Soc. 111 (1989) 1142.
[31] S.K. Doorn, J.T. Hupp, D.R. Porterfield, A. Campion, D.B. Chase, J. Am. Chem. Soc. 112 (1990) 4999.
[32] R.L. Blackbourn, C.S. Johnson, J.T. Hupp, M.A. Bryant, R.L. Sobocinski, J.E. Pemberton, J. Phys. Chem. 95 (1991) 10535.
[33] J.I. Zink, K.S.K. Shin, Adv. Photochem. 16 (1991) 119.
[34] A.B. Myers, Chem. Rev. 96 (1996) 911.
[35] Y.J. Yan, S. Mukamel, J. Chem. Phys. 86 (1987) 6085.
[36] B. Li, A.E. Johnson, S. Mukamel, A.B. Myers, J. Am. Chem. Soc. 116 (1994) 11039.
[37] W. Bensch, M. Prelati, W. Ludwig, J. Chem. Soc., Chem. Commun. (1986) 1762.
[38] C.-M. Che, L.G. Butler, H.B. Gray, R.M. Crooks, W.H. Woodruff, J. Am. Chem. Soc. 105 (1983) 5492.
[39] R.F. Dallinger, V.M. Miskowski, H.B. Gray, W.H. Woodruff, J. Am. Chem. Soc. 103 (1981) 1595.
[40] D. Perreault, M. Drouin, P.D. Harvey, Inorg. Chem. 32 (1993) 1903.
[41] P.D. Harvey, Coord. Chem. Rev. 153 (1996) 175.
[42] S.D. Conradson, A.P. Sattelberger, W.H. Woodruff, J. Am. Chem. Soc. 110 (1988) 1309, also see supporting information of [45].
[43] A.E. Stiegman, S.F. Rice, H.B. Gray, V.M. Miskowski, Inorg. Chem. 26 (1987) 1112.
[44] D. Perreault, M. Drouin, A. Michel, V.M. Miskowski, W.P. Schaefer, P.D. Harvey, Inorg. Chem. 31 (1992) 695.
[45] V.M. Miskowski, S. Franzen, A.P. Shreve, M.R. Ondrias, S.E. Wallace-Williams, M.E. Barr, W.H. Woodruff, Inorg. Chem. 38 (1999) 2546.
[46] B.-H. Xia, C.M. Che, D.L. Phillips, K.H. Leung, K.K. Cheung, Inorg. Chem. 41 (2002) 3866.
[47] B.H. Xia, H.-X. Zhang, C.-M. Che, K.H. Leung, D.L. Phillips, N. Zhu, Z.-Y. Zhou, J. Am. Chem. Soc. 125 (2003) 10362.
[48] W.M. Kwok, C. Zhao, Y.L. Li, X. Guan, D. Wang, D.L. Phillips, J. Am. Chem. Soc. 126 (2004) 3119.